Phosphine-Oxide-Containing Bipolar Host Material for Blue Electrophosphorescent Devices

Fang-Ming Hsu, Chen-Han Chien, Ping-I Shih, and Ching-Fong Shu*

Department of Applied Chemistry, National Chiao Tung University, 300 Hsinchu, Taiwan

Received August 13, 2008. Revised Manuscript Received January 21, 2009

We report highly efficient blue electrophosphorescent organic light-emitting diodes (OLEDs) incorporating a bipolar host, 2,7-bis(diphenylphosphine oxide)-9-(9-phenylcarbazol-3-yl)-9-phenylfluorene (**PCF**), doped with iridium(III) bis[(4,6-difluorophenyl)pyridinato-*N*,$C^{2'}$]picolinate (FIrpic). **PCF**, which contains diphenylphosphine oxide groups appended onto a carbazole/fluorene hybrid, displays both electron- and hole-transporting characteristics, resulting in a low turn-on voltage (2.6 V) and greatly improved power efficiencies. In addition, the sterically hindered structure of **PCF** provides a compatible environment for the FIrpic dopant, alleviating concentration quenching of the phosphor at high doping levels. The device doped with 28 wt % FIrpic exhibited maximum EL efficiencies of 30.8 cd/A and 26.2 lm/W (at 121 cd/m^2). Even at a high brightness of 1000 cd/m^2, the efficiencies remained high (26.9 cd/A and 19.6 lm/W).

Introduction

Organic light-emitting diodes (OLEDs) are receiving much attention for their applications in full-color flat-panel displays and as light sources.[1−7] Efficient commercial OLEDs of the future will most likely incorporate organometallic phosphors because they can harvest both singlet and triplet excitons to achieve nearly 100% internal quantum efficiency.[8−16] Unfortunately, the emission lifetimes of these transition metal complexes are relatively long, leading to undesired triplet−triplet (T_1-T_1) annihilation during the operation of a device.[17] To overcome this problem, researchers commonly dope triplet emittersinto the organic host materials. An ideal host material would meet the following intrinsic requirements: (i) a triplet energy gap (E_T) larger than that of the triplet dopant to prevent reverse energy transfer from the guest back to the host; (ii) good carrier transporting properties to balance the charge flux and reduce the driving voltage; (iii) thermal and morphological stability to extend the device's operational lifetime. Recently, green[18,19] and red[20−23] phosphorescent OLED devices have been developed that exhibit satisfactory EL efficiencies. In contrast, highly efficient blue-light-emitting phosphorescent devices remain rare, mainly because of the lack of suitable host materials possessing both charge transporting characteristics and high triplet energies (E_T).

In this paper, we report blue electrophosphorescent OLEDs incorporating 2,7-bis(diphenylphosphine oxide)-9-(9-phenylcarbazol-3-yl)-9-phenylfluorene (**PCF**) as the host matrix doped with the blue-light triplet emitter iridium(III) bis[(4,6-difluorophenyl)pyridinato-*N*,$C^{2'}$]picolinate (FIrpic). **PCF** exhibits three important features: (i) bipolarity, resulting from the presence of the electron-accepting phosphine oxide moieties[24−29] appended to the carbazole/fluorene hybrid,

* Corresponding author. E-mail: shu@cc.nctu.edu.tw.

(1) Tang, C. W.; VanSlyke, S. A. *Appl. Phys. Lett.* **1987**, *51*, 913.
(2) Service, R. F. *Science* **1996**, *273*, 878.
(3) Shi, J.; Tang, C. W. *Appl. Phys. Lett.* **1997**, *70*, 1665.
(4) Friend, R. H.; Gymer, R. W.; Holmes, A. B.; Burroughes, J. H.; Marks, R. N.; Taliani, C.; Bradley, D. D. C.; Dos Santos, D. A.; Brédas, J. L.; Lögdlund, M.; Salaneck, W. R. *Nature* **1999**, *397*, 121.
(5) Justin Thomas, K. R.; Lin, J. T.; Tao, Y. T.; Chuen, C. H. *Chem. Mater.* **2004**, *16*, 5437.
(6) D'Andrade, B. W.; Forrest, S. R. *Adv. Mater.* **2004**, *16*, 1585.
(7) Service, R. F. *Science* **2005**, *310*, 1762.
(8) Baldo, M. A.; O'Brien, D. F.; You, Y.; Shoustikov, A.; Sibley, S.; Thompson, M. E.; Forrest, S. R. *Nature* **1998**, *395*, 151.
(9) Baldo, M. A.; Lamansky, S.; Burrows, P. E.; Thompson, M. E.; Forrest, S. R. *Appl. Phys. Lett.* **1999**, *75*, 4.
(10) Adachi, C.; Kwong, R. C.; Djurovich, P.; Adamovich, V.; Baldo, M. A.; Thompson, M. E.; Forrest, S. R. *Appl. Phys. Lett.* **2001**, *79*, 2082.
(11) Adachi, C.; Baldo, M. A.; Thompson, M. E.; Forrest, S. R. *J. Appl. Phys.* **2001**, *90*, 5048.
(12) Holmes, R. J.; Forrest, S. R.; Tung, Y. J.; Kwong, R. C.; Brown, J. J.; Garon, S.; Thompson, M. E. *Appl. Phys. Lett.* **2003**, *82*, 2422.
(13) Tokito, S.; Iijima, T.; Suzuri, Y.; Kita, H.; Tsuzuki, T.; Sato, F. *Appl. Phys. Lett.* **2003**, *83*, 569.
(14) Holmes, R. J.; D'Andrade, B. W.; Forrest, S. R.; Ren, X.; Li, J.; Thompson, M. E. *Appl. Phys. Lett.* **2003**, *83*, 3818.
(15) Ren, X.; Li, J.; Holmes, R. J.; Djurovich, P. I.; Forrest, S. R.; Thompson, M. E. *Chem. Mater.* **2004**, *16*, 4743.
(16) Yeh, S. J.; Wu, M. F.; Chen, C. T.; Song, Y. H.; Chi, Y.; Ho, M. H.; Hsu, S. F.; Chen, C. T. *Adv. Mater.* **2005**, *17*, 285.
(17) Baldo, M. A.; Adachi, C.; Forrest, S. R. *Phys. Rev. B* **2000**, *62*, 10967.
(18) Su, S. J.; Chiba, T.; Takeda, T.; Kido, J. *Adv. Mater.* **2008**, *20*, 2125.
(19) Tanaka, D.; Sasabe, H.; Li, Y. J.; Su, S. J.; Takeda, T.; Kido, J *Jpn. J. Appl., Phys.* **2007**, *46*, L10.
(20) Tsuzuki, T.; Tokito, S. *Adv. Mater.* **2007**, *19*, 276.
(21) Okada, S.; Okinaka, K.; Iwawaki, H.; Furugori, M.; Hashimoto, M.; Mukaide, T.; Kamatani, J.; Igawa, S.; Tsuboyama, A.; Takiguchi, T.; Ueno, K. *Dalton Trans.* **2005**, 1583.
(22) Wellmann, P.; Hofmann, M.; Zeika, O.; Werner, A.; Birnstock, J.; Meerheim, R.; He, G.; Walzer, K.; Pfeiffer, M.; Leo, K. *J. Soc. Inf. Disp.* **2005**, *13*, 393.
(23) Birnstock, J.; Canzler, T.; Hofmann, M.; Lux, A.; Murano, S.; Wellmann, P.; Werner, A. *J. Soc. Inf. Disp.* **2008**, *16*, 221.
(24) Padmaperuma, A. B.; Sapochak, L. S.; Burrows, P. E. *Chem. Mater.* **2006**, *18*, 2389.
(25) Vecchi, P. A.; Padmaperuma, A. B.; Qiao, H.; Sapochak, L. S.; Burrows, P. E. *Org. Lett.* **2006**, *8*, 4211.
(26) Burrows, P. E.; Padmaperuma, A. B.; Sapochak, L. S.; Djurovich, P.; Thompson, M. E. *Appl. Phys. Lett.* **2006**, *88*, 183503.
(27) Rehmann, N.; Hertel, D.; Meerholz, K.; Becker, H.; Heun, S. *Appl. Phys. Lett.* **2007**, *91*, 103507.
(28) Cai, X.; Padmaperuma, A. B.; Sapochak, L. S.; Vecchi, P. A.; Burrows, P. E. *Appl. Phys. Lett.* **2008**, *92*, 083308.

10.1021/cm802199d CCC: $40.75
Published on Web 02/19/2009

thereby facilitating both electron and hole injection and transport; (ii) a value of E_T that remains as high as 2.75 eV, resulting from the individual building blocks being connected through a nonconjugated linkage (the sp^3-hybridized C-9 atom of fluorene); and (iii) a sterically bulky and hindered structure, capable of inhibiting the aggregation of guest emitters and providing excellent thermal stability (glass-transition temperature (T_g): 147 °C). Taken together, these features make **PCF** an appropriate host for blue phosphorescent dopants, such as FIrpic (E_T = 2.62 eV).

Experimental Section

Materials. 2,7-Dibromo-9-phenyl-9-fluorenol (**1**)[30] and 9-(9-phenylcarbazol-3-yl)-9-phenylfluorene[31] were prepared according to reported procedures. Solvents were dried using standard methods. All other reagents were used as received from commercial sources, unless stated otherwise.

Characterization. ^{1}H, ^{13}C, and ^{31}P NMR spectra were recorded on Varian UNITY INOVA 500 MHz and Varian UNITY 300 MHz spectrometers. Mass spectra and high-resolution mass spectra (HRMS) were obtained using JEOL JMS-HX 110 and Finnigan Thermo Quest MAT 95XL mass spectrometers, respectively. Differential scanning calorimetry (DSC) was performed using a SEIKO EXSTAR 6000DSC unit operated at a heating rate of 10 °C/min and a cooling rate of 50 °C/min; the glass transition temperatures (T_g) were determined from the second heating scan. Thermogravimetric analysis (TGA) was undertaken using a DuPont TGA 2950 instrument; the thermal stability of the sample was determined under a nitrogen atmosphere by measuring the weight loss while heating at a rate of 20 °C/min. UV−vis spectra were measured using an HP 8453 diode-array spectrophotometer. PL spectra were obtained using a Hitachi F4500 luminescence spectrometer. The low-temperature phosphorescence spectrum was obtained using a composite spectrometer incorporating a monochromator (Jobin Yvon, Triax 190) coupled with a liquid nitrogen-cooled charge-coupled device (CCD) detector (Jobin Yvon, CCD-1024 × 256-open-1LS). Cyclic voltammetry (CV) measurements were performed using a BAS 100 B/W electrochemical analyzer operated at a scan rate of 100 mV/s. The potentials were measured against an Ag/Ag^+ (0.01 M $AgNO_3$) reference electrode. The highest occupied molecular orbital (HOMO) energies of organic thin films were measured using a photoelectron spectrometer (Riken-Keili AC-2). Atomic force microscopy measurements were performed in the tapping mode under ambient conditions using a Digital Nanoscope IIIa instrument.

Fabrication of OLEDs. The EL devices were fabricated through vacuum deposition of the materials at 1 × 10^{-6} torr onto indium tin oxide (ITO) glass having a sheet resistance of 25 Ω/square. All of the organic layers were deposited at a rate of 1.0 Å/s. The cathode was completed through thermal deposition of LiF (15 Å) at a deposition rate of 0.1 Å/s; it was then capped with Al metal (100 nm) through thermal evaporation at a rate of 4.0 Å/s. The current−voltage-luminance relationships of the devices were measured using a Keithley 2400 source meter and a Newport 1835C optical meter equipped with an 818ST silicon photodiode. The EL spectrum was obtained using a Hitachi F4500 luminescence spectrometer.

Synthetic Procedures. *2,7-Dibromo-9-(9-phenylcarbazol-3-yl)-9-phenylfluorene (**2**).* CF_3SO_3H (2.14 mL, 24.4 mmol) was added dropwise to a mixture of 9-phenylcarbazole (5.92 g, 24.3 mmol) and **1** (5.04 g, 12.1 mmol) in dichloromethane (100 mL). This mixture was stirred under nitrogen for 30 min at room temperature before being quenched with saturated aqueous $NaHCO_3$ (100 mL). The organic phase was washed twice with water (100 mL) and then dried ($MgSO_4$). Evaporation of the volatiles resulted in a yellowish crude product, which was purified through column chromatography (SiO_2; ethyl acetate/hexane, 1:10) to afford **2** as a white solid (3.74 g, 48%). ^{1}H NMR (300 MHz, $CDCl_3$) δ 8.00 (d, J = 7.8 Hz, 1H), 7.85 (d, J = 1.8 Hz, 1H), 7.64 (s, 1H), 7.61 (s, 2H), 7.59−7.42 (m, 9H), 7.38 (d, J = 3.6 Hz, 2H) 7.32−7.21 (m, 5H), 7.19 (dd, J = 8.7, 1.8 Hz, 2H). ^{13}C NMR (75 MHz, $CDCl_3$) δ 154.03, 145.44, 141.57, 140.31, 138.39, 137.86, 136.27, 131.23, 130.20, 129.87, 128.91, 128.41, 127.84, 127.50, 127.33, 126.66, 126.46, 123.59, 123.41, 122.21, 121.96, 120.78, 120.29, 119.70, 110.29, 110.17, 66.10. MS (EI) *m/z*: 641 [M^+].

*2,7-Bis(diphenylphosphine oxide)-9-(9-phenylcarbazol-3-yl)-9-phenylfluorene (**PCF**).* *n*-Butyllithium (2.5 M in hexane, 3.40 mL, 8.50 mmol) was added dropwise to a stirred solution of **2** (2.61 g, 4.07 mmol) in anhydrous tetrahydrofuran (200 mL) under a nitrogen atmosphere at −78 °C. After the solution was stirred at −78 °C for an additional 3 h, chlorodiphenylphosphine (1.58 mL, 8.59 mmol) was added to provide a clear, pale-yellow solution. The mixture was warmed gradually to room temperature over 4 h while stirring continuously. The reaction was quenched through the addition of water (200 mL) and the mixture was then extracted with ethyl acetate (2 × 100 mL). The combined extract was dried ($MgSO_4$) and then concentrated under the reduced pressure. The crude product was dissolved in dichloromethane (150 mL) and then 30% aqueous hydrogen peroxide (30 mL) was added. The mixture was stirred at room temperature for 3 h and then extracted with dichloromethane (3 × 50 mL). The collected organic phase was dried ($MgSO_4$) and then concentrated under reduced pressure. The residue was purified through column chromatography (SiO_2; ethyl acetate/methanol, 50:1) to yield **PCF** as a white solid (2.56 g, 71%). ^{1}H NMR (300 MHz, THF-d_8) δ 8.05 (dd, J = 7.8, 2.4 Hz, 2H), 7.93 (s, 2H), 7.89 (s, 2H), 7.82−7.74 (m, 4H), 7.69−7.53 (m, 12H), 7.48−7.41 (m, 5H), 7.38−7.33 (m, 10H), 7.21−7.11 (m, 8H). ^{13}C NMR (75 MHz, THF-d_8) δ 153.72 (d, $J_{C,P}$ = 12.1 Hz), 147.14, 143.91, 142.67, 141.38, 139.19, 137.81, 135.61 (d, $J_{C,P}$ = 101.6 Hz), 135.53 (d, $J_{C,P}$ = 101.7 Hz), 133.34 (d, $J_{C,P}$ = 9.5 Hz), 133.12 (d, $J_{C,P}$ = 10.0 Hz), 132.83, 131.69 (d, $J_{C,P}$ = 10.5 Hz), 131.69, 129.70 (d, $J_{C,P}$ = 11.6 Hz), 129.67 (d, $J_{C,P}$ = 11.5 Hz), 129.23, 128.92, 128.36, 128.25, 128.04, 127.38, 124.69, 124.63, 122.57, 122.40, 121.76, 121.19, 120.17, 111.29, 111.00, 67.28. ^{31}P NMR (202 MHz, THF-d_8) δ 24.23. HRMS (FAB, *m/z*): calcd for $C_{61}H_{44}NO_2P_2$ [M + H]$^+$, 884.2847; found, 884.2856.

Results and Discussion

Synthesis. Scheme 1illustrates the synthetic route followed for the preparation of the bipolar host material **PCF**. The starting material, 2,7-dibromo-9-phenyl-9-fluorenol (**1**), was synthesized as reported previously.[30] We prepared 2,7-dibromo-9-(9-phenylcarbazol-3-yl)-9-phenylfluorene (**2**) through the acid-promoted Friedel−Crafts-type substitution of **1** with excess 9-phenylcarbazole. Lithiation of **2** with *n*-butyllithium and subsequent treatment with chlorodiphenylphosphine gave a phosphine-containing intermediate, which we oxidized with 30% aqueous hydrogen peroxide to yield the target molecule **PCF**. We characterized the structure of **PCF** using ^{1}H, ^{13}C,

(29) Sapochak, L. S.; Padmaperuma, A. B.; Cai, X.; Male, J. L.; Burrows, P. E. *J. Phys. Chem. C* **2008**, *112*, 7989.
(30) Chien, C. H.; Shih, P. I.; Wu, F. I.; Shu, C. F.; Chi, Y. *J. Polym. Sci., Part A: Polym. Chem.* **2007**, *45*, 2073.
(31) Shih, P. I.; Chiang, C. L.; Dixit, A. K.; Chen, C. K.; Yuan, M. C.; Lee, R. Y.; Chen, C. T.; Diau, E. W. G.; Shu, C. F. *Org. Lett.* **2006**, *8*, 2799.

Scheme 1

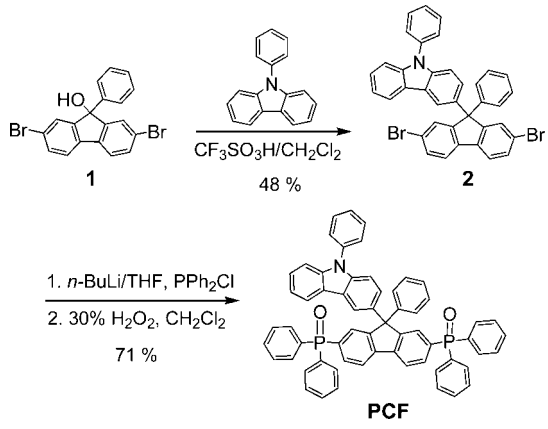

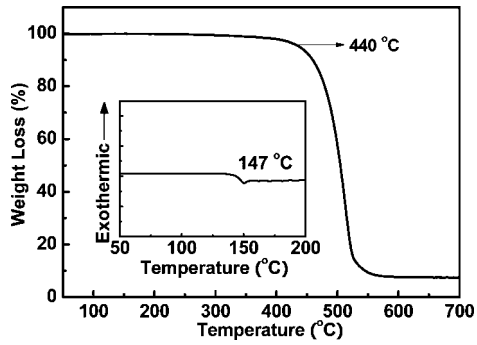

Figure 1. TGA thermogram of **PCF** recorded at a heating rate of 20 °C/min. The inset displays the DSC trace of **PCF** collected at a heating rate of 10 °C/min.

and ^{31}P NMR spectroscopy and high-resolution mass spectrometry.

Thermal Properties. We used differential scanning calorimetry (DSC) and thermogravimetric analysis (TGA) to investigate the thermal properties of **PCF**. Under DSC examination, **PCF** revealed a distinct glass transition at 147 °C (inset to Figure 1). The presence of its diphenylphosphine oxide moieties renders **PCF** rather bulky and rigid, leading to a significant enhancement in amorphous stability relative to that of its phosphine oxide-free counterpart, 9-(9-phenylcarbazol-3-yl)-9-phenylfluorene (**CF**; T_g = 108 °C).[31] Because joule heating is inevitable under the conditions of device operation, the higher thermal resistance of **PCF** makes it a feasible host material to improve the lifetime of OLED devices. **PCF** also exhibits high thermochemical stability, as evidenced by its TGA 5%-weight-loss temperature under a nitrogen atmosphere being as high as 440 °C (Figure 1). As reported previously, the presence of triarylphosphine oxide moieties incorporated into engineered polymers imparts high thermal and chemical stability.[32] The high value of $T_d^{5\%}$ suggested to us that **PCF** was thermally stable and would be capable of enduring vacuum thermal sublimation for OLED fabrication.

Photophysical Properties. Figure 2a depicts the room-temperature absorption and PL spectra of **PCF** in various solutions. The absorption spectra in cyclohexane, THF, and CH_3CN are almost identical, i.e., independent of the solvent

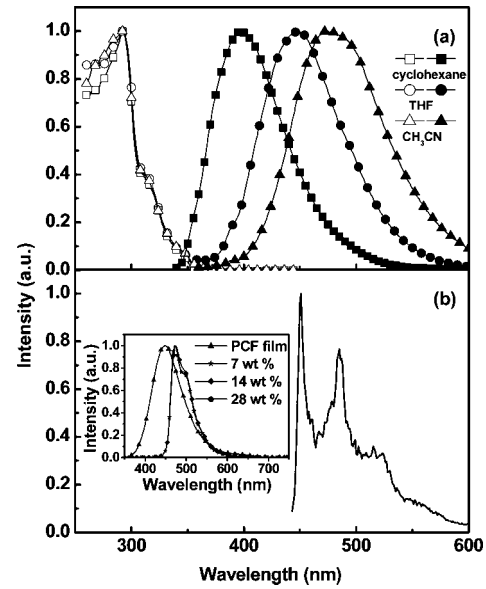

Figure 2. (a) Room-temperature absorption and PL spectra of **PCF** in various organic solvents (excited at 330 nm). (b) Phosphorescence spectrum of **PCF** in a frozen 2-methyltetrahydrofuran matrix at 77 K (excited at 330 nm). The inset displays the PL spectrum of a **PCF** film [formed on quartz substrates by thermal evaporation (30 nm), excited at 330 nm] and the EL spectra of FIrpic-doped**PCF** devices at various doping concentrations.

polarity, implying that the Franck−Condon excited-state is subject to a rather small dipolar change with respect to the ground state. On the other hand, the signals in the photoluminescence spectra shifted significantly to longer wavelength upon increasing the solvent polarity. We attribute this phenomenon to a mechanism involving rapid photoinduced electron transfer between the carbazole donor and the phosphine oxide-substituted fluorene acceptor units, resulting in a large change in the dipole moment in the excited state; a subsequent solvent relaxation process leads to the solvent polarity-dependent emission.[33,34] When we plotted the emission peak frequencies of **PCF** in various organic solvents (from cyclohexane to acetonitrile) as a function of solvent polarities, we obtained a linear relationship together with a slope as steep as $-14\,500$ cm^{-1}, consistent with our assignment of a charge-transfer emission (see Figure S1 in the Supporting Information).[33,34] Moreover, when we varied the concentration of **PCF** in THF solutions over the range from 1×10^{-4} to 1×10^{-6} M, we observed that the intensities of the absorption at 330 nm (originated from the carbazole moiety) and the emission at 446 nm were linearly proportional to the studied concentrations. These results suggest that we can eliminate the possibility of the emission resulting from an aggregation effect. In the spectra of **CF**, which contains solely the carbazole electron donor, we observed, accordingly, a negligible shift in the position of the emission signal with respect to the solvent polarity. From Figure 2b, we estimated the value of E_T of **PCF** to be 2.75 eV, as determined by taking the highest-energy 0−0 phos-

(32) Watson, K. A.; Palmieri, F. L.; Connell, J. W. *Macromolecules* **2002**, *35*, 4968.

(33) Chien, Y. Y.; Wong, K. T.; Chou, P. T.; Cheng, Y. M. *Chem. Commun.* **2002**, 2874.

(34) Wong, K. T.; Ku, S. Y.; Cheng, Y. M.; Lin, X. Y.; Hung, Y. Y.; Pu, S. C.; Chou, P. T.; Lee, G. H.; Peng, S. M. *J. Org. Chem.* **2006**, *71*, 456.

(35) Kolosov, D.; Adamovich, V.; Djurovich, P.; Thompson, M. E.; Adachi, C. *J. Am. Chem. Soc.* **2002**, *124*, 9945.

Table 1. Physical Properties of PCF **and** CF

	λ_{abs}[a] (nm)			λ_{em} (nm)							
host	*c*-Hex	THF	CH_3CN	*c*-Hex	THF	CH_3CN	E_T (eV)	E_g (eV)	HOMO[d] (eV)	LUMO[e] (eV)	T_g (°C)
PCF	293, 312, 345	293,312,345	292, 312, 345	396	446	472	2.75	3.10[b]	−5.86	−2.76	147
CF	297, 310, 348	298,310,348	297, 309, 348	353, 367	357, 372	358, 372	2.88	3.44[c]	−5.87	−2.43	108

[a] Measured in cyclohexane (*c*-Hex), tetrahydrofuran (THF), and acetonitrile (CH_3CN).; [b] On the basis of electrochemical results. [c] Estimated from the optical absorption threshold. [d] Measured using a Riken-Keiki AC-2 photoelectron spectrometer. [e] Calculated by adding the energy gaps to the HOMO energies.

phorescent emission measured in a frozen 2-methyltetrahydrofuran matrix at 77 K. The value of E_T of **PCF**, which was higher than that of the conventional triplet blue dopant FIrpic (2.62 eV), was sufficient for it to serve as a suitable host. The inset to Figure 2b presents the PL spectrum of a **PCF** film and the EL spectra of FIrpic-doped**PCF** devices at various doping concentrations. For the 7 wt %-doped device, we observe only the FIrpic emission, indicating the complete energy transfer from **PCF** to FIrpic. Even when the doping level was as high to 28 wt %, the emission spectrum remained identical to that of the 7 wt %-doped device, with no exciplex or excimer emissions occurring.

Electrochemical Properties. We investigated the electrochemical properties of **PCF** and **CF** through CV using a Ag/Ag^+ (0.01 M $AgNO_3$) reference electrode. Upon cathodic sweeping in tetrahydrofuran, **PCF** exhibited one reversible reduction with an onset potential of −2.11 V, originating from the fluorene unit substituted with phosphoryl groups. In contrast, the donor-only compound **CF** revealed no reduction wave in the cathodic scan up to −3.10 V. During the anodic scan in dichloromethane, **PCF** and **CF** displayed similar oxidation processes, with onset potentials of 0.99 and 0.97 V, respectively, that derived from the electron-rich carbazole pendent group.

The HOMO energy levels of **PCF** and **CF**, measured using a photoelectron spectrometer (Riken-Keiki AC-2), were −5.86 and −5.87 eV, respectively. These similar values imply that the HOMO energy levels were affected mainly by the carbazole moieties in the **PCF** and **CF** molecules. We obtained the lowest unoccupied molecular orbital (LUMO) energy levels for **PCF** and **CF** by adding the corresponding energy band gaps (E_gs) to the HOMO energies. Because the oxidation and reduction behavior within the bipolar **PCF** derive from the electron-rich carbazole and electron-deficient phosphorylfluorene functionalities, we used the energy band gap (3.10 eV) estimated from the electrochemistry measurements to calculate the LUMO level (−2.76 eV). In the case of the unipolar **CF**, we employed the optical band gap (3.44 eV) obtained from the absorption threshold of the carbazole group to estimate the LUMO energy level (−2.43 eV). Table 1 lists the key data relating to the energy levels.

Electroluminescence Properties of OLEDs. We fabricated blue light-emitting devices having the configuration indium tin oxide (ITO)/9,9-bis[4-(*N*,*N*-diphenylamino)phenyl]fluorene (BPAF, 30 nm)/*x* wt % FIrpic:host (30 nm)/3-(4-biphenylyl)-4-phenyl-5-(4-*tert*-butylphenyl)-1,2,4-triazole (TAZ, 40 nm)/LiF (15 Å)/Al (100 nm), where the host was either **PCF** or its phosphine oxide-free counterpart **CF**;[31]

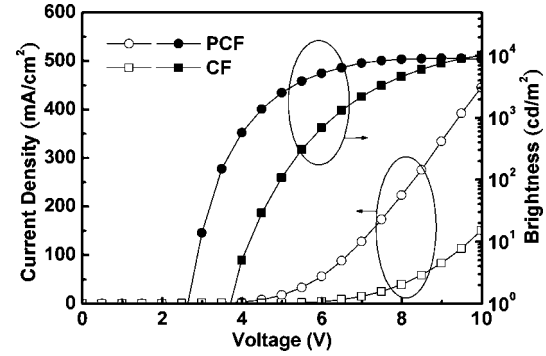

Figure 3. Current density and brightness plotted with respect to applied voltage for **PCF**- and **CF**-based devices doped with 7 wt % FIrpic.

we employed BPAF[36] and TAZ as hole- and electron-transporting layers that would also confine the excitons within the emissive layer. To verify the role played by the diphenylphosphine oxide units in **PCF**, we compared the behavior of the **PCF**- and **CF**-based devices that were both doped with 7 wt % FIrpic. As revealed in Figure 3, the current density of the **PCF**-based device was considerably higher than that of its **CF** counterpart under the same applied voltage. We ascribe the steeper current density−voltage (*I*−*V*) curve of the former device to the presence of the diphenylphosphine oxide moieties, which furthermore facilitate electron injection and transport within the **PCF** host, rather than the injection and transport of holes alone within **CF**. The peak external quantum efficiency of the **PCF** device was 9.6%, relatively higher than that of the **CF** device (8.6%). More importantly, the lower operating voltage resulted in the **PCF** device demonstrating an almost 2-fold enhancement in its maximum power efficiency (17.2 lm/W) in comparison to that of the **CF**-based device (8.8 lm/W).

To compare the charge injection properties of **PCF** and **CF**, we investigated the *I*−*V* characteristics of hole-only devices having the configuration ITO/BPAF (30 nm)/host (30 nm)/BPAF (40 nm)/Al (100 nm) and electron-only devices having the configuration ITO/2,9-dimethyl-4,7-diphenyl-1,10-phenanthroline (BCP, 30 nm)/host (30 nm)/TAZ (40 nm)/LiF (15 Å)/Al (100 nm). In the case of hole-only devices, no electron injection occurred from the Al cathode to the BPAF layer because of the low electron affinity (EA) of BPAF (2.00 eV). Only holes could be injected from the anode; they then passed through the organic layers without any light emission originating from the organic layers. On the other hand, BCP, which possesses a large ionization potential (IP) of 6.50 eV, acted as a hole-blocker to inhibit the injection of holes from the ITO anode to the BCP layer. Therefore, only electrons were injected into the

(36) El-Khouly, M. E. *Spectrochim. Acta, Part A* **2007**, *67*, 636.

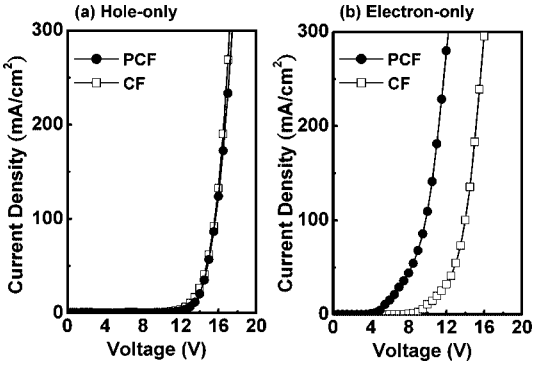

Figure 4. Current density−voltage ($I-V$) characteristics of (a) hole- and (b) electron-only devices.

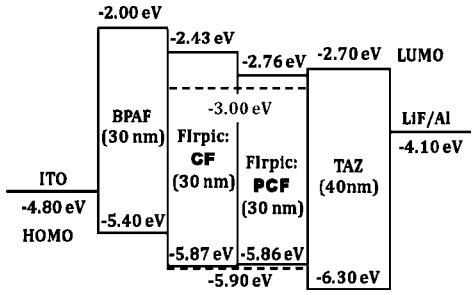

Figure 5. Relative HOMO/LUMO energy levels of the materials used for the EL devices.

organic layers in the electron-only devices. The hole-only devices incorporating **PCF** and **CF** exhibited similar $I-V$ curves (Figure 4a); thus, the introduction of the diphenylphosphine oxide groups did not alter the hole injection capabilities, which resulted mainly from the presence of the carbazole donor units. In contrast, the **PCF**-based electron-only device possessed a significantly lower threshold voltage and a higher current density than its **CF** counterpart under the same bias (Figure 4b). Because the estimated LUMO level for **PCF** (−2.76 eV) was 0.33 eV lower than that of **CF** (−2.43 eV; Figure 5), the energy barrier for electron injection from TAZ to the **PCF** layer was considerably lower than that to the **CF** layer. As a result, electron injection was facilitated in the **PCF**-based device.[24−29]

According to literature reports,[14,37] the EL efficiency is often strongly dependent on the concentration of the triplet dopant. Hence, for optimization of the performance of the **PCF**-based devices, we varied the doping concentration of FIrpic from 7 to 28 wt %. As indicated in Figure 6a, the $I-V$ characteristics of our **PCF**-based devices doped with different concentrations of FIrpic were nearly identical, implying that the charge injection in the emissive layer did not change. The phenomenon can be explained by considering the energy level diagrams of the devices (Figure 5), in which the HOMO/LUMO energy levels of **PCF** were close to that of FIrpic. Thus, the carrier-injection barriers from the hole- and electron-transporting layers to either **PCF** or FIrpic were almost identical. Consequently, the increasing concentration of FIrpic did not significantly alter the degree of charge injection in the emissive layer. In contrast, the brightnesses of these devices all increased significantly upon

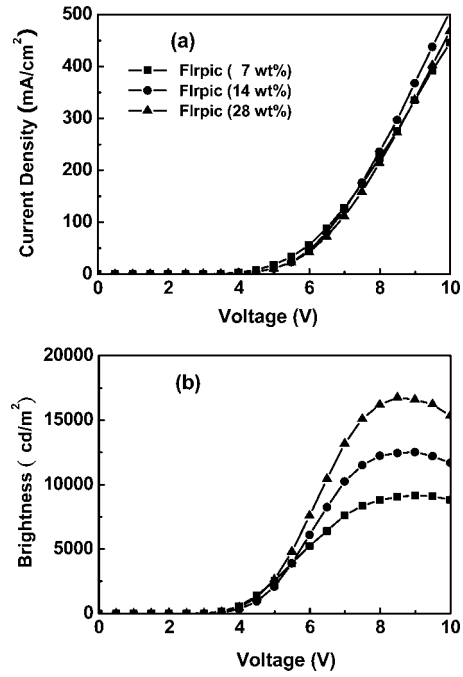

Figure 6. (a) Current density−voltage ($I-V$) and (b) brightness−voltage ($L-V$) characteristics of **PCF**-based devices doped with various concentrations of FIrpic.

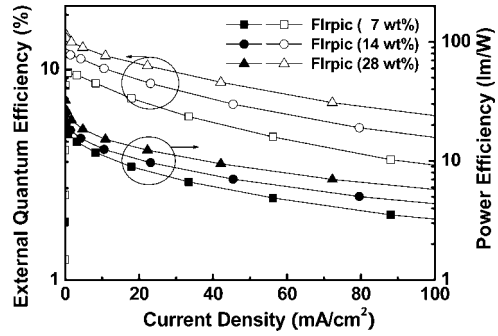

Figure 7. Efficiency-current density characteristics for **PCF**-based devices doped with various concentrations of FIrpic.

increasing the concentration of FIrpic (Figure 6b). The EL efficiencies were, therefore, improved dramatically upon increasing the concentration of the dopant (Figure 7), providing the maximum external quantum efficiency and power efficiency of 14.8% and 26.2 lm/W (at 121 cd/m^2) when 28 wt % FIrpic was present. Note that these efficiencies, which remained at 13.0% and 19.6 lm/W, respectively, when we increased the brightness up to 1000 cd/m^2, are among the highest levels reported for blue phosphorescent OLEDs.[38−43] Table 2 summarizes the key characteristics of our various FIrpic-doped devices.

(37) Li, W.; Qiao, J.; Duan, L.; Wang, L.; Qiu, Y. *Terahedron* **2007**, *63*, 10161.
(38) Tsai, M. H.; Lin, H. W.; Su, H. C.; Ke, T. H.; Wu, C. C.; Fang, F. C.; Liao, Y. L.; Wong, K. T.; Wu, C. I. *Adv. Mater.* **2006**, *18*, 1216.
(39) Tsai, M. H.; Hong, Y. H.; Chang, C. H.; Su, H. C.; Wu, C. C.; Matoliukstyte, A.; Simokaitiene, J.; Grigalevicius, S.; Grazulevicius, J. V.; Hsu, C. P. *Adv. Mater.* **2007**, *19*, 862.
(40) Whang, D. R.; You, Y.; Kim, S. H.; Jeong, W. I.; Park, Y. S.; Kim, J. J.; Park, S. Y. *Appl. Phys. Lett.* **2007**, *91*, 233501.
(41) Lin, J. J.; Liao, W. S.; Huang, H. J.; Wu, F. I.; Cheng, C. H. *Adv. Funct. Mater.* **2008**, *18*, 485.
(42) Su, S. J.; Sasabe, H.; Takeda, T.; Kido, J. *Chem. Mater.* **2008**, *20*, 1691.
(43) Tanaka, D.; Agata, Y.; Takeda, T.; Watanabe, S.; Kido, J *Jpn. J. Appl., Phys.* **2007**, *46*, L117.

Table 2. Performance of PCF- and CF-Based Devices

	PCF			CF		
	7 wt % FIrpic	14 wt % FIrpic	28 wt % FIrpic	7 wt % FIrpic	14 wt % FIrpic	28 wt % FIrpic
$V_{\text{turn-on}}$ (V)[a]	2.6	2.6	2.6	3.7	3.7	3.5
$\eta_{\text{ext, max}}$ (%)[b]	9.6	11.9	14.8	8.6	10.7	11.8
$\eta_{\text{c, max}}$ (cd/A)[b]	18.8	23.3	30.8	16.7	20.7	24.2
$\eta_{\text{p, max}}$ (lm/W)[b]	17.2	20.9	26.2	8.8	12.8	14.9
η_{ext} (%)[c]	8.9 (8.4)	11.2 (10.2)	13.0 (11.8)	8.4 (8.0)	10.2 (9.5)	11.7 (11.7)
η_{c} (cd/A)[c]	17.5 (16.3)	22.0 (20.0)	26.9 (24.5)	16.3 (15.6)	19.8 (18.3)	23.9 (23.9)
η_{p} (lm/W)[c]	13.0 (11.2)	15.3 (12.7)	19.6 (15.7)	8.2 (7.4)	10.8 (9.4)	14.4 (13.0)
V (V)[c]	4.3 (4.6)	4.0 (5.0)	4.3 (5.0)	6.2 (6.6)	5.8 (6.2)	5.2 (5.8)
CIE (x, y)[d]	(0.13, 0.32)	(0.14, 0.33)	(0.13, 0.35)	(0.13, 0.32)	(0.14, 0.32)	(0.15, 0.35)

[a] Recorded at 1 cd/m^2. [b] $\eta_{\text{ext, max}}$, maximum external quantum efficiency, $\eta_{\text{c, max}}$, maximum luminance efficiency, $\eta_{\text{p, max}}$, maximum power efficiency. [c] Recorded at 1000 cd/m^2; the data in parentheses were recorded at 10 mA/cm^2. [d] Measured at 7 V.

Generally, when the dopant concentration increases, the probability of carrier recombination at the dopant emitters increases, leading to higher device efficiency. On the other hand, the efficiency may decrease dramatically upon increasing the doping level as a result of triplet−triplet annihilation and concentration quenching effects arising from strong bimolecular interactions of the phosphor. In the case of **PCF**, we speculate that the degree of aggregation between FIrpic molecules may have been reduced significantly; consequently, self-quenching of the Ir phosphor was restrained effectively in the devices. To confirm this hypothesis, we employed atomic force microscopy (AFM) to investigate the surface morphology of the 28 wt % FIrpic-doped **PCF** film. For the purpose of comparison, we also studied the surface morphology of the neat **PCF** film. The AFM images in Figure S2 of the Supporting Information reveal similar homogeneous topographies for the FIrpic-doped and nondoped **PCF** films, with root-mean-square (rms) surface roughnesses of 0.34 and 0.32 nm, respectively. These results reveal that doping 28 wt % FIrpic into **PCF** had a negligible effect on the properties of the film. Thus, the sterically bulky and hindered structure of**PCF** appears to provide an almost ideal stabilizing environment in which the Ir emitters are isolated and dispersed homogeneously, even at a doping concentration as high as 28 wt %. In contrast, the 21 wt % FIrpic-doped film based on the commercial host material 1,3-bis(9-carbazolyl)benzene (mCP), which does not have a bulky and nonplanar structure, displayed some hill-like patterns; its rms surface roughness was 0.63 nm (0.33 nm for the neat film), indicating that the high doping level led to aggregation of the phosphors.[44] This phenomenon, in turn, led to a remarkable decrease in the EL efficiency as a result of the strong bimolecular interactions of the phosphor.

In the case of the **CF**-based devices, the maximum external quantum efficiencies improved from 8.6 to 11.8% and the operating voltages decreased from 6.6 to 5.8 V (at 10 mA/cm^2) when we increased the concentrations of FIrpic from 7 to 28 wt %. Because it is a unipolar, hole-transporting material, **CF** was unable to allow efficient electron injection and transport from the electron-transporting layer. This phenomenon occurred in the electron-only devices (vide supra). Because the LUMO level of FIrpic (−3.00 eV) was significantly lower than that of **CF** (−2.43 eV), electrons had the potential to be trapped at FIrpic. At higher doping levels, more electrons were injected directly to the dopant molecules, which provided an additional channel to transport electrons through hopping between the dopant sites. Accordingly, higher FIrpic concentrations improved the charge balance in the emissive layer and reduced the operating voltage. In addition, AFM images of the 28 wt % FIrpic-doped and nondoped **CF** films revealed similar homogeneous topographies, with rms surface roughnesses of 0.39 and 0.36 nm, respectively. This result indicated that the improved EL efficiency at higher doping levels might possibly be attributed in part to the bulky nature of **CF** host, in which the phosphorescent emitters are isolated and dispersed homogeneously to restrain concentration quenching.

Conclusion

We have prepared highly efficient FIrpic-based blue electrophosphorescent devices incorporating a novel bipolar host material, **PCF**, which features diphenylphosphine oxide groups appended to a carbazole/fluorene hybrid. The favorable bipolar characteristics of **PCF** facilitate both hole and electron injection and transport, leading to significantly lower operating voltages and great improvements in power efficiency when compared to the unipolar **CF** counterpart. In addition, the sterically bulky and hindered molecular structure of **PCF**, as well as **CF,** results in effective suppression of the self-quenching of the Ir phosphor at high doping levels. Subsequently, by increasing the FIrpic concentration to 28 wt %, the **PCF** device exhibited maximum device efficiencies of 14.8% (30.8 cd/A) and 26.2 lm/W. Even at a brightness as high as 1000 cd/m^2, these efficiencies remained at 13.0% (26.9 cd/A) and 19.6 lm/W, respectively. This performance suggests that **PCF** is a potential host material for the development of commercial OLED devices.

Acknowledgment. We thank the National Science Council of the Republic of China for financial support.

Supporting Information Available: A plot of the emission peak frequencies of the **PCF** solutions as a function of the solvent polarity; AFM topographic images of the 28 wt % FIrpic-doped and nondoped **PCF** films (PDF). This material is available free of charge via the Internet at http://pubs.acs.org.

CM802199D

(44) Shih, P. I.; Chien, C. H.; Wu, F. I.; C. F. Shu *Adv. Funct. Mater.* **2007**, *17*, 3514.